Ab Initio Study of Molecular Hydrogen Adsorption in Covalent Organic Framework-1

Pornjuk Srepusharawoot,*,†,‡ Ralph H. Scheicher,† C. Moysés Araújo,† Andreas Blomqvist,† Udomsilp Pinsook,§,∥ and Rajeev Ahuja†,⊥

Condensed Matter Theory Group, Department of Physics and Materials Science, Uppsala University, Box 530, SE-751 21 Uppsala, Sweden, Department of Physics, Faculty of Science, Khon Kaen University, 40002, Khon Kaen, Thailand, Department of Physics, Faculty of Science, Chulalongkorn University, 10330, Bangkok, Thailand, ThEP, Commission on Higher Education, 328 Si-Ayutthaya road, 10400, Bangkok, Thailand, and Applied Materials Physics, Department of Materials and Engineering, Royal Institute of Technology (KTH), SE-100 44 Stockholm, Sweden

Received: October 16, 2008; Revised Manuscript Received: March 6, 2009

The adsorption energies of hydrogen molecules at all possible adsorption sites of covalent organic framework-1 (COF-1) are studied by density functional theory (DFT) and second-order Møller−Plesset perturbation theory (MP2). The most favorable adsorption sites from our DFT results are on the top of an oxygen atom for the B_3O_3 ring and on the top of the center of the C−C bond for the benzene ring when a single H_2 is interacting with the COF-1. The adsorption energy trend obtained from the DFT calculations is found to be in good agreement with the MP2 binding energy trend. The binding preferences are slightly changed when high hydrogen loading is considered. H_2 molecules prefer to be trapped on the top of the carbon atoms of the benzene ring and also on the top of the oxygen atoms of the B_3O_3 ring. These findings are confirmed by hydrogen center-of-mass distribution results obtained using molecular dynamics simulations. Moreover, our DFT results reveal that the hydrogen adsorption energies are boosted when we increase the number of hydrogen loadings due to attractive H_2−H_2 interactions. In addition, the nonavailability of the remaining adsorption sites in the COF-1 leads to a reduction of the H_2 mobility.

I. Introduction

Owing to the risks emerging from a global energy crisis and climate change phenomena, new sustainable energy resources with nontoxic byproducts are sought for use in the near future. Hydrogen is widely discussed as a prominent energy carrier due to its abundance and higher gravimetric energy density than the currently used ordinary energy resources based on fossil fuels.[1,2] Moreover, upon reaction with oxygen in a fuel cell to generate electricity, the only byproduct is water. However, hydrogen gas occupies a large amount of space, which results in the problematic issue of efficient storage in mobile applications. There is a great effort to research suitable hydrogen storage materials for automobile applications with high gravimetric density, fast kinetics, long life cycle times, and favorable thermodynamics.[3] Much evidence exists in the literature that systems possessing benzene-like structures such as graphite,[5,6] graphene,[6,7] carbon nanotubes,[8−10] and metal organic frameworks[11−13] are able to trap hydrogen molecules in the system and could thus act, in principle, as hydrogen storage materials. However, very weak binding interactions between adsorbed H_2 and host materials are the main drawback, resulting in only small amounts (or even none) of adsorbed hydrogen remaining in the host materials at room temperature. For example, the maximum hydrogen gravimetric density of graphite and graphene is about 1.9 and 2.2 wt % respectively at 77 K and ambient pressure.[14]

Because the molecular weight of the host system should be as low as possible to achieve a high H_2 gravimetric density, light elements should be chosen to construct the system. The covalent organic frameworks[16] have been successfully synthesized from light elements such as hydrogen, boron, carbon, and oxygen, forming strong covalent bonds. COF-1 is chosen in the current work due to its comparatively small unit cell and consequently low number of atoms, which results in a reasonable computational cost for our first-principles level calculations. COF-1 exhibits high thermal stability (up to 600 °C) and low density. In addition, COF-1 possesses a permanent porosity with a pore volume of 0.36 cm^3/g.[17] In experiments, the hydrogen storage capacity of the COF-1 was found to be 1.28 wt % at 77 K and ambient pressure.[17] At room temperature and 10 MPa of pressure, the percentage of hydrogen uptake decreases to 0.26 wt %.[17]

The COF-1 framework contains 36 atoms of C, 12 atoms each of O and B, and 24 atoms of H. Its crystal structure belongs to space group P_{63}/mmc with $a = b = 15.6529$ Å and $c = 6.7005$ Å.[16] There are two layers in the unit cell: layer A at $z = c/4$, and layer A′ at $z = 3c/4$. For layer A, each B in the boroxine (B_3O_3) rings is connected to the benzene (C_6H_4) rings, forming a periodic framework. The crystal structure of the layer A′ is identical to layer A but it is rotated by 60° and shifted by the translational vector $\vec{r} = (1/3)\hat{i} - (1/3)\hat{j}$, where $\hat{i}$ and $\hat{j}$ correspond to the unit vectors along the x and y directions, respectively. The crystal structure of the COF-1 is illustrated in Figure 1.

II. Computational Details

Total-energy calculations and ab initio molecular dynamics simulations were carried out within the framework of DFT[18,19] as implemented in the Vienna Ab initio Simulation Package

* Corresponding author. E-mail: pornjuk.srepusharawoot@fysik.uu.se.
† Uppsala University.
‡ Khon Kaen University.
§ Chulalongkorn University.
∥ ThEP, Commission on Higher Education.
⊥ Royal Institute of Technology (KTH).

10.1021/jp809167b CCC: $40.75
Published on Web 04/16/2009

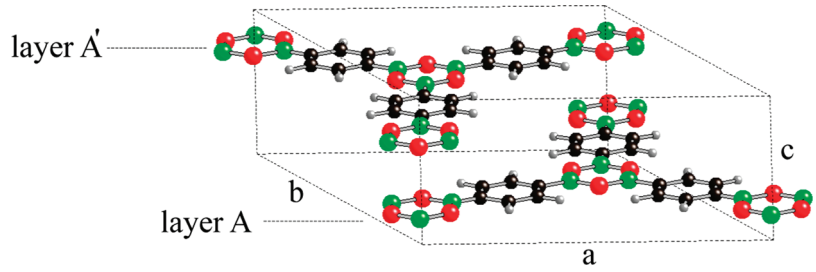

Figure 1. The COF-1 unit cell. Green, red, black, and gray spheres represent B, O, C and H atoms, respectively. The lattice constants along lattice vectors $\vec{a}_1$, $\vec{a}_2$, and $\vec{a}_3$ are labeled as a, b, and c, respectively.

(VASP).[20] The projector augmented wave method (PAW)[21] was used and the valence states of the PAW potentials are 2s2p for B, C, and O, and 1s for H. A high cutoff energy of 1400 eV for the plane waves was found to achieve convergence. Because of the large system size of the primitive cell and the nature of the electronic structure, it was sufficient to employ k-points sampling at the Γ-point only. Ionic positions and unit cell parameters were optimized with the conjugate−gradient algorithm with forces acting between the ions evaluated from the Hellmann−Feynman theorem. We performed ab initio molecular dynamics simulations at temperatures of 77, 150, and 300 K. The time step used in all calculations is 1 fs and the velocities are rescaled for every time step. To determine the suitable exchange correlation functional for the system, the COF-1 structural parameters evaluated from both local density approximation (LDA)[22] and generalized gradient approximation (GGA)[23] types of exchange correlation functional were compared to the experimental results, and we found that the COF-1 structural parameters obtained from the LDA functional are in better agreement with the experimental results than those from the GGA functional. Of course, just as with any standard DFT functional, LDA is not well suited to describe systems bound by van der Waals interaction as it will lead to severe overbinding. However, LDA was shown to be able to predict the trend of hydrogen molecule physisorption energies in substantial agreement with experiments, for example for graphene and carbon nanotubes, where LDA and the second-order Møller−Plesset perturbation theory (MP2) calculations of the hydrogen physisorption energy on planar graphitic clusters[24] were compared with each other and it was found that the LDA interaction energy curve is in very good qualitative agreement with the MP2 calculations. In addition, we have shown in our previous work[25] that the LDA functional can produce the experimental trend for the hydrogen adsorption energy at the metal oxide cluster of MOF-5. Therefore, as long as one always remembers that the absolute binding energy values obtained from LDA can be dramatically too high, and only regards the *trend* in binding energies as reliable, it is appropriate to use the LDA exchange correlation functional for the qualitative study of van der Waals-bound systems. With this cautiousness in mind, we have employed LDA in the present work.

A much more reliable approach for the calculation of van der Waals-dominated binding energies is the above-mentioned MP2 method. The drawback is that this method is computationally much more demanding than LDA, so the application to large systems is generally impossible due to prohibitively large requirements for computational resources and time. Nevertheless, we attempted to reach a more accurate understanding of the binding energies by using the MP2 method as implemented in *Gaussian 03*[26] with the 6-311G** basis set. Because of the previously stated reasons, it is practically impossible to study the full periodic COF-1 system. An often chosen compromise is then to take into account only a small cluster of the system to lower the computational expense to an acceptable level, and this is the approach we adapted. The MP2 binding energy results reported here by us have been corrected for the basis set superposition error (BSSE) with the counterpoise correction method.[27,28]

III. Results and Discussion

To obtain the minimum energy ground-state configuration, the COF-1 crystal structure was fully optimized without any symmetry constraint. The calculated parameters of the COF-1 were determined by us as follows: lattice constants $a = b =$ 14.99 Å and $c = 6.03$ Å, corresponding to an interlayer distance of 3.02 Å. O−B and B−C bond lengths were found to be 1.38 and 1.54 Å, respectively. These results are in perfect agreement with measurements obtained in triphenylboroxine.[29] The computed B−O−B and O−B−O angles are 121.9 and 118.2°, respectively. Here again, we found excellent agreement with triphenylboroxine studies,[29] the deviation between the experimental results and our theoretical values being only 0.2°.

For investigating the hydrogen adsorption sites, we looked at the adsorption sites of graphene as a model.[6] According to the model, a hydrogen molecule is introduced on top of an oxygen atom, on top of a boron atom of the B_3O_3 ring, and on top of a carbon atom of the benzene rings, referred to as oxygen site, boron site, and carbon site, respectively. Moreover, it is possible to trap H_2 at the center of a B−O bond in the B_3O_3 ring or at the center of a C−C bond in the benzene ring, both labeled as bridge sites. The hollow sites at the center of the boroxine or benzene rings are yet another possible H_2 adsorption site in the COF-1 system. We also note that an H_2 molecule can be adsorbed at the bridge site of a B−C bond in COF-1. The calculated binding energy for that site is roughly the same as that for the boron site. For small concentrations of H_2 in the system, this is therefore indeed a likely trapping site; however, for higher levels of hydrogen loading it will be somewhat problematic for H_2 to stay at the B−C bridge site due to the repulsive interaction from H_2 occupying the adjacent carbon sites. It was for this reason that the bridge site of the B−C bond is neglected in this work.

To determine the hydrogen binding energies at the various identified adsorption sites, the adsorption energy of the hydrogen molecules was calculated by us as follows:

$$\Delta E_B = E(\text{COF-1}) + nE(H_2) - E(\text{COF-1}{:}nH_2)$$

where $E(\text{COF-1}{:}nH_2)$, $E(\text{COF-1})$, and $E(H_2)$ are the total energies of the COF-1 framework containing n adsorbed H_2 molecules, the intrinsic COF-1 framework, and a free H_2 molecule, respectively. Because the main goal of our present study is to obtain binding energy *trends*, we neglected the contribution from vibrational and rotational energies of H_2. The

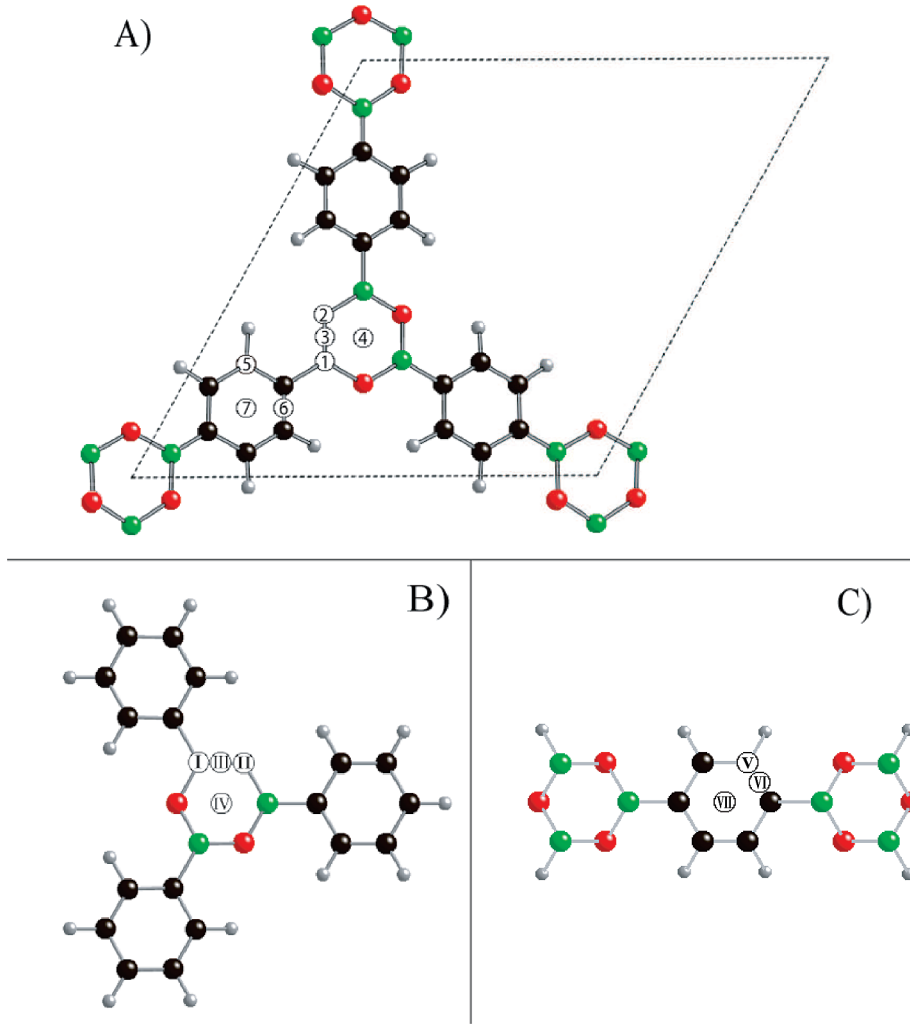

Figure 2. A) Hydrogen adsorption sites in COF-1. Numbers 1−7 correspond to the different sites as follows: 1 boron site, 2 oxygen site, 3 and 4 bridge and hollow sites of the B_3O_3 ring, respectively, 5 carbon site, and 6 and 7 bridge and hollow sites of benzene ring, respectively. B) The roman numerals I, II, III, and IV denote the adsorption sites of the B_3O_3 cluster for our MP2 calculations and refer to the boron site, oxygen site, bridge, and hollow sites, respectively. C) The roman numerals V, VI, and VII indicate trapping sites of the C_6H_4 cluster in the following order: carbon site, bridge, and hollow sites.

adsorption energies of the hydrogen molecule were calculated for the following sites: for the B_3O_3 ring, at an oxygen site, at a boron site, at bridge and hollow sites; for the benzene ring, at a carbon site, at bridge and hollow sites as shown in part A of Figure 2. The studied cluster system and positions of the adsorption sites of B_3O_3 and C_6H_4 rings for the MP2 part of our investigation are represented in parts B and C of Figure 2. Results for all adsorption sites are presented for the head-on configuration (which has the axis of the H_2 molecule aligned in parallel with the *c* axis of the COF-1 system), since we found from total energy calculations that the head-on orientation always resulted in a higher binding energy than the parallel configuration (in which the axis of the H_2 molecule lies in a plane parallel to the plane formed by the *a* and *b* axes of the COF-1 system). Furthermore, our molecular dynamics simulations confirm this finding as they have also revealed that the head-on configuration is clearly favored over the parallel one. The binding energies corresponding to the adsorption sites are displayed as bar graphs in Figure 3.

On the basis of our DFT calculations, the most favorite adsorption site on the B_3O_3 ring, when only a single H_2 is present in the system, is on the oxygen site, followed by bridge, boron, and hollow sites, respectively. Hydrogen adsorption energies obtained from MP2 calculations yield an exactly identical trend

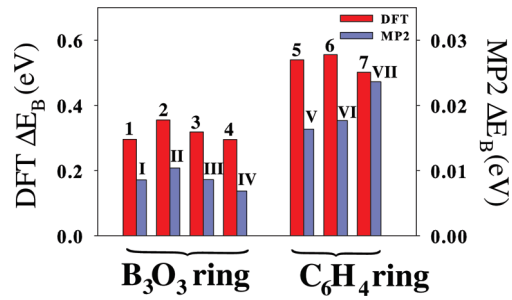

Figure 3. Binding energies of a single hydrogen molecule on a boron site, an oxygen site, a carbon site, on bridge and hollow sites on B_3O_3 and C_6H_4 rings (a detailed description of these sites are provided in the text and in the schematic shown in Figure 2). The dark-red and light-blue bars refer to the hydrogen adsorption energies at the above adsorption sites of B_3O_3 and C_6H_4 rings as calculated by DFT and MP2 methods, respectively.

with the DFT results. For the benzene ring, the most stable adsorption site in DFT calculations is the bridge site, followed by carbon site and hollow site, whereas the binding energy trend from MP2 calculations differs slightly from the DFT binding energy trend, namely, hollow > bridge > carbon site. This disagreement can be explained as follows: the close proximity between hollow site and layer A′ in the DFT calculation results

in a stronger repulsive interaction between the atoms of layer A′ and H_2 molecule compared to other adsorption sites because the A′ layer is not included in the MP2 cluster calculations, the corresponding repulsive effect at the hollow site is absent, resulting in the different binding energy trend.

By comparing the DFT adsorption energies between graphene (Supporting Information) and COF-1 systems, the H_2 binding energies in COF-1 are found to be relatively high compared to graphene because the interaction between H_2 and COF-1 framework is not only due to the weak dispersive interaction but also due to electrostatic interaction between the H_2 quadrupole moment and the charge states of B and O atoms in the B_3O_3 ring and of C in the benzene ring adjacent to B. To quantitatively determine the amount of charge on these atoms, we have carried out Bader charge analysis[30] of the full periodic COF-1 system and found that the charge states of O, B, and the C atom adjacent to B, are O^{2-}, B^{3+} and C^{1-}, respectively, whereas the other carbon atoms and hydrogen atoms including those of the adsorbed H_2 are essentially in the neutral state. When we introduce a hydrogen molecule to the framework, the charges of the framework interact with the permanent quadrupole of the hydrogen molecule, resulting in electrostatic interactions between the framework and the H_2 molecule. The lower H_2 binding energies at the B_3O_3 ring are due to the repulsive interaction between B^{3+} of layer A and the adsorbed H_2, whereas this interaction is rather small in case of a H_2 molecule staying on the benzene ring of layer A. Moreover, the interaction between the COF-1 host and an adsorbed H_2 is not only from the interaction from layer A but also from layer A′. To clarify this effect, we have calculated the DFT-LDA binding energies for the two following cases: (i) deleting layer A and keeping both layer A′ and H_2 molecule at the given adsorption site, and (ii) removing layer A′ and keeping layer A and H_2 molecule at the given adsorption site. Our results reveal that approximately 96.5% and 91.7% of the total H_2 binding energies come from the interaction between the layer A and adsorbed H_2 when a hydrogen molecule sits at B_3O_3 and C_6H_4 rings, respectively. Moreover, our results also show that the binding energies of the benzene ring are higher than those of the boroxine ring for both cases.

As it can be seen in Figure 3, our MP2 binding energies are comparable to the results obtained for H_2 physisorbed on graphene (Supporting Information) and they would be even further increased (approximately by a factor of 2) when taking into account the contributions to the interaction energy from the repeated layer A and to a lesser extent from layer A′. In addition, the employed cluster size will also affect the binding energy, with more extended clusters generally yielding larger binding energies (Supporting Information and ref 4). From our DFT-LDA results, we find that the dominating part of the total binding energy comes from the interaction between layer A and adsorbed H_2. Only relatively small contributions of the total binding energy originate from the interaction between layer A′ and adsorbed H_2. Thus, because our results show that the interaction from layer A is in fact the major contribution, the MP2 adsorption energy trend (which takes H_2 interaction with a cluster representation of layer A into account) should be regarded as representative for the actual COF-1 system. As shown in Figure 3, the LDA adsorption energy trend follows closely that of the much more reliable MP2 results. This is in agreement with the expectation stated in section II, namely that LDA can yield a qualitatively correct behavior of the binding energy, whereas the quantitative behavior can be wrong even by one order of magnitude. We therefore interpret the result as support for the view that the H_2 binding energy trend obtained from DFT-LDA calculations may be quite reliable for this particular system, even though the absolute binding energy values are certainly too high due to the known overbinding issues of LDA.

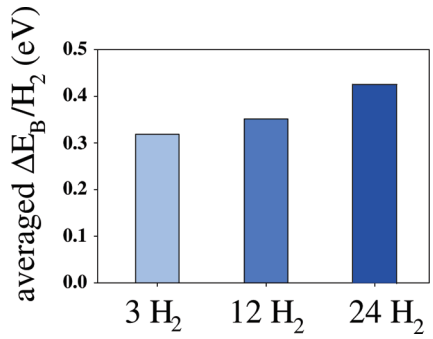

Figure 4. Averaged hydrogen physisorption energy in COF-1 per H_2 of nH_2 (n = 3, 12, and 24).

The equilibrium distance between the center of mass of the adsorbed H_2 and the framework falls in the range from 2.7 to 3.0 Å, almost equal to the interlayer distance between layer A and A′ of COF-1. In other words, the H_2 molecules are located in the pore hole of that layer A′. When 3 H_2 molecules are introduced to the system, we averaged the binding energies obtained from the H_2 molecules being either distributed over the oxygen sites of the B_3O_3 ring or over three alternating carbon sites of the benzene ring. This averaging process was necessary to allow for a meaningful comparison with the subsequent cases of 12 H_2 and 24 H_2 molecules present because, in those latter cases, H_2 molecules are distributed over sites in both the B_3O_3 ring and the benzene ring. The averaged binding energies per H_2 in the case of 3 H_2 molecules were found to be almost indifferent to the case when a single H_2 is present in the system. By analyzing the density of states data of the COF-1 with 1 H_2 and 3 H_2, we found that the density of states of the combined system is virtually identical to the superposition of the individual densities of states of the COF-1 framework and free hydrogen molecules. Moreover, we also tested for the following three cases: 3 H_2 distributed over (i) boron sites, (ii) B−O bridge sites, and (iii) C−C bridge sites. Our results reveal however that these three configurations are unstable configurations; hydrogen is observed to move to the above two sites, namely an oxygen site in the case of being initially placed on a B−O bridge, and a carbon site when placed initially on a boron site, and finally on a C−C bridge when a full optimization has been carried out.

Because of the rather high adsorption energy in the 3 H_2 case, it appears feasible to stabilize more than three H_2 molecules in the COF-1 structure. In the current work, we have investigated putting 12 H_2 and 24 H_2 molecules into the COF-1 system. For the 12 H_2 case, 3 H_2 were placed at an oxygen site of the B_3O_3 ring and 3 H_2 were inserted at a carbon site of each benzene ring of the layer A. We also placed 12 H_2 at both the layer A and A′ in the case referred to as the 24 H_2 case. As we observe in Figure 4, the averaged binding energies per H_2 are seen to rise as an increment of the number of hydrogen loading from 3 H_2 to 24 H_2. These results show that the H_2 configuration leads to an attractive H_2-H_2 interaction in this system.

To understand the effects of H_2-H_2 interactions when the number of hydrogen molecules increases from 3 H_2 to 12 H_2, we performed ab initio molecular dynamics simulations of n H_2 with n = 1, 3, 12, and 24 at temperatures of 77, 150, and 300 K. For the 1 H_2 case, we initially placed H_2 at an oxygen site of the B_3O_3 ring and the bridge site of the C_6H_4 ring because these sites had yielded the highest binding energies in our DFT

studies. From an analysis of the hydrogen molecule trajectory at 77 K, it is seen that the H_2 moves to the nearest benzene ring when we initially place it at an oxygen site of the B_3O_3 ring. This is due to the higher binding energy of the adsorption site at the benzene ring than that at the B_3O_3 ring. Expectedly, an H_2 remains trapped at the benzene ring when we initially put an H_2 at a bridge site of the benzene ring.

For the case of 3 H_2 molecules, each H_2 was placed at an oxygen site. We found that all hydrogen molecules were able to remain trapped at their initial sites because of the attractive H_2-H_2 interaction. When 3 H_2 molecules are placed at carbon sites of the C_6H_4 ring, the H_2 molecules are repelled to move away from their initial adsorption sites by the H atoms of C_6H_4 from the layer A′ (because the adsorbed H_2 are in a pore at the same height as the layer A′). As a result, one H_2 molecule is seen to move to the nearest B_3O_3 ring and the rest is able to trap on the C_6H_4 ring, that is one H_2 molecule is trapped on the initial benzene ring and another H_2 molecule is bounded to the adjacent C_6H_4 ring.

Upon a further increase of the number of hydrogen molecules loaded to the COF-1 system from 3 H_2 to 12 H_2 or 24 H_2, all H_2 molecules were found to be capable to remain trapped at the initial sites, that is, 3 H_2 at the oxygen sites of the B_3O_3 ring and 9 H_2 at the carbon sites of the C_6H_4 rings for the 12 H_2 case, or 6 H_2 at the oxygen sites of B_3O_3 rings and 18 H_2 at the carbon sites of the C_6H_4 rings for the 24 H_2 case. In the current work, we calculated the time-averaged hydrogen density distribution at 77 K to confirm the hydrogen configuration obtained from zero Kelvin total energy calculation in case of 24 H_2 loading in the COF-1. The hydrogen density distribution, $\rho(\vec{x})$, at any given time is defined as

$$\rho(\vec{x}) = \begin{cases} \sum_i \exp -\frac{1}{2}\left(\frac{|\vec{x}-\vec{R}_i|}{\sigma}\right)^2 & , \quad |\vec{x}-\vec{R}_i| \le 3\sigma \\ 0 & , \quad |\vec{x}-\vec{R}_i| > 3\sigma \end{cases}$$

where $\vec{R}_i$ is the position of center of mass of the i^{th} hydrogen molecule and $\sigma = 0.5$ Å.[31] By plotting the internal energy versus time, we were able to conclude that thermal equilibrium is reached within 400 time steps or 0.4 ps. After thermal equilibrium has been reached, the hydrogen distribution of COF-1 was averaged over a time interval of 2.5 ps at 77 K. The resulting plot is displayed in Figure 5.

According to Figure 5, our hydrogen distribution result is absolutely in agreement with the total energy DFT results. In addition, we found that hydrogen molecules are able to stay at the oxygen sites of the B_3O_3 ring and approximately on the carbon sites of the benzene rings. This is due to the fact that there remain no available adsorption sites in both B_3O_3 and benzene rings resulting in reduction of the H_2 mobilities. As a result, H_2 molecules are able to stay on their initial adsorption sites and increase the averaged binding energies as shown in Figure 4. However, at the benzene ring, H_2 is not exactly trapped on top of the carbon atoms because of the repulsion between H atoms of the C_6H_4 ring from the layer A′ and adsorbed H_2. Consequently, the adsorbed H_2 is slightly shifted away from the carbon site (c.f., Figure 5).

When the simulation temperature is increased to 150 K, a single inserted H_2 molecule is observed to become more mobile due to having many available adsorption sites at the B_3O_3 and C_6H_4 rings, which H_2 can access. This situation also occurs in the case of inserting 3 H_2 at the oxygen sites of the B_3O_3 ring. When we initially introduce 3 H_2 at the carbon sites of the C_6H_4 ring, the H_2 molecules that are close to the H atoms from the C_6H_4 in the layer A′ are repelled from the initial adsorption site, resulting in one H_2 still staying at the initial site in the original C_6H_4 ring, whereas the other 2 H_2 are pushed to the adjacent C_6H_4 rings. However, we find that H_2 molecules can stay at their initial sites, both oxygen site and carbon site, in the cases of 12 H_2 and 24 H_2 in the system. This result confirms that the unavailability of binding sites for adsorbing H_2 molecules leads to decreased H_2 mobility, resulting in sitting of hydrogen molecules at a given adsorption site.

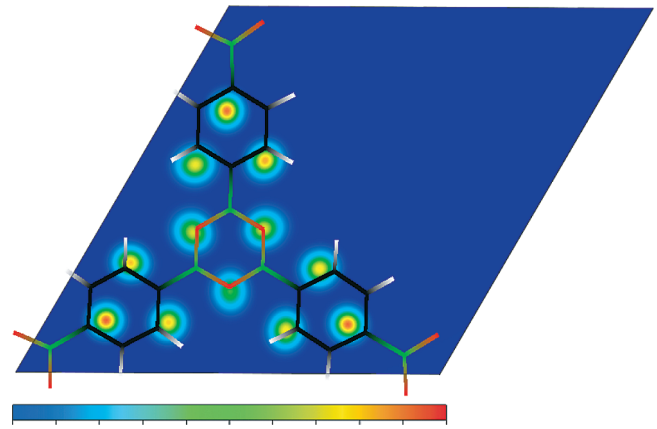

Figure 5. Time-averaged hydrogen molecule center of mass distribution in the (001) plane at $T = 77$ K. For the sake of clarity, we display only the hydrogen distribution in the layer A at $z = 3.8$ Å. The distribution in the layer A′ was found to be qualitatively identical. The colors specify the magnitude of the H_2 distribution and change on a linear scale from blue (corresponding to zero hydrogen density) to red (corresponding to the highest recorded hydrogen density). The colors identifying the various elements of the COF-1 framework are identical to those used in Figure 1.

At room temperature (300 K), H_2 molecules are seen to move around the COF-1 framework for both 1 H_2 and 3 H_2 cases. In the case of introducing 12 H_2 and 24 H_2 in the COF-1, we found that only a few hydrogen molecules detach from the adsorption sites. This again confirms our previous observation that repulsive short-range H_2-H_2 interaction leads to a reduced H_2 mobility and thus plays an important role in stabilizing H_2 to remain trapped on their adsorption sites.

As it can be seen from the trajectory plot in Figure 6, H_2 molecules are indeed rather mobile within the COF-1 framework. This can be understood from the fact that the kinetic energy of the H_2 molecules is on the same order of magnitude or even higher than the energy barriers typically encountered in the potential energy surface between the adjacent adsorption sites. When traveling between adjacent trapping sites, H_2 is not required to desorb but stays actually close to the sheets in COF-1 (part B of Figure 6), switching gradually from one trapping site to another. Briefly put, the energy barrier between the carbon site and the bridge site in C_6H_4 can be estimated to approximately 0.016 eV. The energy barriers between boron site and B−O bridge site and between oxygen site and B−O bridge site in the B_3O_3 ring are about 0.022 and 0.037 eV, respectively. These small energy barriers can then be overcome quite easily by H_2 molecules jumping from one trapping site to another.

According to the Bader analysis of self-consistent charge density,[30] the charge states of O, B, and C, which is adjacent to B in the COF-1, are O^{2-}, B^{3+}, and C^{1-}, respectively, and the rest of carbons and hydrogens are in the neutral state. Hence, there exists the electrostatic interactions between quadrupole of adsorbed H_2 molecule and the COF-1 framework. Finally, these results lead to the conclusion that the attraction between

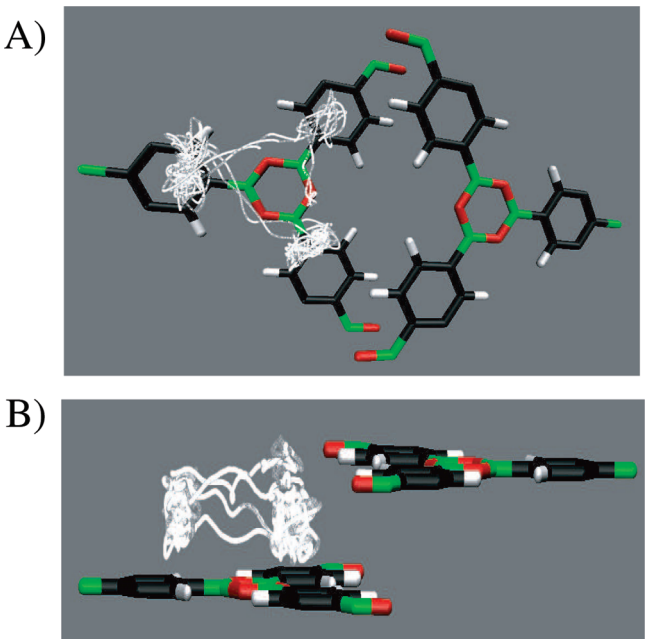

Figure 6. The trajectories of the H atoms of a single H_2 molecule obtained at 150 K from ab initio molecular dynamics simulation are shown in white here. A) Top view. B) Side view.

an adsorbed H_2 and COF-1 host should be due to the combination of weak dispersive interactions and electrostatic interactions.

IV. Conclusions

We performed extensive total energy calculations and ab initio molecular dynamics simulations based DFT and MP2 to systematically study the H_2 physisorption energies corresponding to all possible adsorption sites for COF-1, namely oxygen site, boron site, bridge, and hollow sites of the B_3O_3 ring and carbon site, bridge, and hollow sites of benzene ring. Our DFT studies showed that the head-on orientation of H_2 leads to stronger binding than the parallel orientation of H_2. By placing a single H_2 in the COF-1, the trend of adsorption energies obtained from DFT calculations is found to be in good agreement with our MP2 calculations. However, from a quantitative point of view, our benchmark calculations for H_2 physisorption on graphene indicate that the MP2 binding energies for H_2 in COF-1 appear to be more reliable than those obtained from DFT. Hydrogen molecules are preferably adsorbed at the oxygen sites of the B_3O_3 ring and at the carbon site of benzene ring when the number of hydrogen loading in the system is increased. This result is confirmed by our hydrogen density distribution result. When we increase the number of hydrogen loading to 3 H_2, 12 H_2, and 24 H_2, we found that the binding energy rises with the number of hydrogen loading, showing the effect of the attractive H_2-H_2 interaction. Our ab initio molecular dynamics simulations at 77, 150, and 300 K also revealed that the unavailability of H_2 adsorption sites in the system can reduce the hydrogen mobility resulting in trapping of H_2 at a given adsorption site, a consequence of the repulsive short-range H_2-H_2 interaction. On the basis of the results from the Bader charge analysis of self-consistent charge density, the interaction between COF-1 and adsorbed hydrogen appears to consist of a combination between the weak dispersive and the electrostatic forces.

Finally, whereas our study has shown from first principles that COF-1 can indeed act as a hydrogen storage material at very low temperatures, the issue remains how the binding energy could be enhanced, so that a large wt % of H_2 could be stored at ambient conditions in the system. Clearly, further investigations into improved designs are required to tackle this problem for COF-1. One possible approach might be again to dope the system with light alkali metals, such as Li, which can create charged centers that bind H_2 much more strongly, as was for example shown by us[15] for MOF-5. Recently, Mulfort et al.[32] have used the reduction method for adding Li in the metal organic frameworks (MOFs) by combining the MOF sample with the solvent mixing Li metal in dimethylformamide. We believe that this method might be a promising path toward experimentally synthesizing light-metal decorated COFs.

Acknowledgment. We gratefully acknowledge STINT, VR, Futura, Göran Gustafsson Stiftelse, Wenner-Gren Stiftelserna, and the Thailand Research Fund (TRF) for financial support, as well as SNIC and UPPMAX for providing computing time.

Supporting Information Available: Binding energy equation, graphs of binding energies versus distance, drawing of graphene cluster used in MP2 calculations, and table of binding energies. This material is available free of charge via the Internet at http://pubs.acs.org.

References and Notes

(1) Schlapbach, L.; Züttel, A. *Nature.* **2001**, *414*, 353–358.
(2) Conte, M.; Iacobazzi, A.; Ronchetti, M.; Vellone, R. *J. Power Sources* **2001**, *100*, 171–187.
(3) http://www1.eere.energy.gov/hydrogenandfuelcells/storage
(4) Heine, T.; Zhechkov, L.; Seifert, G. *Phys. Chem. Chem. Phys.* **2004**, *6*, 980–984.
(5) Chambers, A.; Park, C.; Baker, R. T. K.; Rodriguez, N. M. *J. Phys. Chem. B* **1998**, *102*, 4253–4256.
(6) Arellano, J. S.; Molina, L. M.; Rubio, A.; Alonso, J. A. *J. Chem. Phys.* **2000**, *112*, 8114–8119.
(7) Patchkovskii, S.; Tse, J. S.; Yurchenko, S. N.; Zhechkov, L.; Heine, T.; Seifert, G. *Proc. Natl. Acad. Sci. U.S.A.* **2005**, *102*, 10439–10444.
(8) Dillon, A. C.; Jones, K. M.; Bekkedahl, T. A.; Kiang, C. H.; Bethune, D. S.; Heben, M. J. *Nature (London)* **1997**, *386*, 377–379.
(9) Liu, C.; Fan, Y. Y.; Liu, M.; Cong, H. T.; Cheng, H. M.; Dresselhaus, M. S. *Science* **1999**, *286*, 1127–1129.
(10) Yildirim, T.; Ciraci, S. *Phys. Rev. Lett.* **2005**, *94*, 175501.
(11) Eddaoudi, M.; Kim, J.; Rosi, N.; Vodak, D.; Watcher, J.; OKeeffe, M.; Yaghi, O. M. *Science* **2002**, *295*, 469–472.
(12) Rosi, N. L.; Eckert, J.; Eddaoudi, M.; Vodak, D. T.; Kim, J.; OKeeffe, M.; Yaghi, O. M. *Science* **2003**, *300*, 1127–1129.
(13) Yildirim, T.; Hartman, M. R. *Phys. Rev. Lett.* **2005**, *95*, 215504.
(14) Touzik, A.; Hermann, H. *Chem. Phys. Lett.* **2005**, *416*, 137–141.
(15) Blomqvist, A.; Moysés Araújo, C.; Srepusharawoot, P.; Ahuja, R. *Proc. Natl. Acad. Sci. U.S.A.* **2007**, *104*, 20173–20176.
(16) Côté, A. P.; Benin, A. I.; Ockwig, N. W.; OKeeffe, M.; Matzger, A. J.; Yaghi, O. M. *Science* **2005**, *310*, 1166–1170.
(17) Li, Y.; Yang, R. T. *AIChE J.* **2008**, *54*, 269–279.
(18) Kohn, W.; Sham, L. J. *Phys. Rev.* **1965**, *140*, A1133−A1138.
(19) Hohenberg, P.; Kohn, W. *Phys. Rev.* **1964**, *136*, B864−B871.
(20) Kresse, G.; Furthmüller, J. *Phys. Rev. B* **1996**, *54*, 11169–11186.
(21) Blöchl, P. E. *Phys. Rev. B* **1994**, *50*, 17953–17979.
(22) Ceperley, D. M.; Alder, B. J. *Phys. Rev. Lett.* **1980**, *45*, 566–569.
(23) Perdew, J. P.; Burke, K.; Ernzerhof, M. *Phys. Rev. Lett.* **1996**, *77*, 3865–3868.
(24) Okamoto, Y.; Miyamoto, Y. *J. Phys. Chem. B* **2001**, *105*, 3470–3474.
(25) Srepusharawoot, P.; Moysés Araújo, C.; Blomqvist, A.; Scheicher, R. H.; Ahuja, R. *J. Chem. Phys.* **2008**, *129*, 164104.
(26) Frisch, M. J.; Trucks, G. W.; Schlegel, H. B.; Scuseria, G. E.; Robb, M. A.; Cheeseman, J. R.; Montgomery, J. A., Jr.; Vreven, T.; Kudin, K. N.; Burant, J. C.; Millam, J. M.; Iyengar, S. S.; Tomasi, J.; Barone, V.; Mennucci, B.; Cossi, M.; Scalmani, G.; Rega, N.; Petersson, G. A.; Nakatsuji, H.; Hada, M.; Ehara, M.; Toyota, K.; Fukuda, R.; Hasegawa, J.; Ishida, M.; Nakajima, T.; Honda, Y.; Kitao, O.; Nakai, H.; Klene, M.; Li, X.; Knox, J. E.; Hratchian, H. P.; Cross, J. B.; Bakken, V.; Adamo, C.; Jaramillo, J.; Gomperts, R.; Stratmann, R. E.; Yazyev, O.; Austin, A. J.; Cammi, R.; Pomelli, C.; Ochterski, J. W.; Ayala, P. Y.; Morokuma, K.; Voth, G. A.; Salvador, P.; Dannenberg, J. J.; Zakrzewski, V. G.; Dapprich, S.; Daniels, A. D.; Strain, M. C.; Farkas, O.; Malick, D. K.; Rabuck, A. D.; Raghavachari, K.; Foresman, J. B.; Ortiz, J. V.; Cui, Q.; Baboul, A. G.; Clifford, S.; Cioslowski, J.; Stefanov, B. B.; Liu, G.; Liashenko, A.; Piskorz,

P.; Komaromi, I.; Martin, R. L.; Fox, D. J.; Keith, T.; Al-Laham, M. A.; Peng, C. Y.; Nanayakkara, A.; Challacombe, M.; Gill, P. M. W.; Johnson, B.; Chen, W.; Wong, M. W.; Gonzalez, C.; Pople, J. A.; *Gaussian 03*, Rev. C.02; Gaussian, Inc.: Wallingford, CT, 2004.

(27) Simon, S.; Duran, M.; Dannenberg, J. J. *J. Chem. Phys.* **1996**, *105*, 11024–11031.

(28) Boys, S. F.; Bernardi, F. *Mol. Phys.* **1970**, *19*, 553–566.

(29) Brock, C. P.; Minton, R. P.; Niedenzu, K. *Acta Crystallogr. C* **1987**, *43*, 1775–1779.

(30) Henkelman, G.; Arnaldsson, A.; Jónsson, H. *Comput. Mater. Sci.* **2006**, *36*, 354–360.

(31) Mueller, T.; Ceder, G. *J. Phys. Chem. B* **2005**, *109*, 17974–17983.

(32) Mulfort, K. L.; Hupp, J. T. *J. Am. Chem. Soc.* **2007**, *129*, 9604–9605.

JP809167B